Development of a New Type-I Isotherm for Correction of Langmuir Isotherm's Over-Estimation of Adsorption at Higher Pressures

ABSTRACT

Different gas equilibrium adsorption models (or isotherms) with various theoretical frameworks have been applied to quantify adsorbed volume (V) of gas (or fluid) through pressure-volume behaviour at constant temperature. Most often, Langmuir isotherm (representing Type I Isotherm) has been used in modelling monolayer adsorption despite the fact that it yields over-estimation at higher pressures thus contradicting the description of Type I isotherm. Here, higher pressures refer to pressures above the adsorption saturation pressure (P_s).

Hence, in this work, a new Type I adsorption isotherm involving pressure (P), adsorption saturation pressure (P_s), maximum adsorbed volume (V_{max}), and adsorbate-adsorbent resistance parameter (n) was developed using kinetic approach. The developed adsorption isotherm is: $V = \begin{Bmatrix} V_{max}\left\{\frac{P}{P_s} + \left(1 - \frac{P}{P_s}\right)\left(\frac{P}{P_s}\right)^n\right\}, for\ P < P_s \\ V_{max},\ for\ P \geq P_s \end{Bmatrix}$ and it shows that V_{max} is attained when pressure increases to P_s, above which no further gas adsorption occurs. The developed isotherm can be used to model all cases of monolayer adsorptions of gases (or fluids) on adsorbents.

The developed and Langmuir isotherms were used in modelling secondary low-pressure gas adsorption data of different adsorbents, and the qualities of fit were statistically assessed. For laboratory methane adsorption on Turkey's shale sample at 25 ^{o}C, the developed isotherm yields a correlation with R^2 value of 0.997 and predicts a maximum adsorption volume of 0.0450 mmol/g at a P_s of 2,005 psia. However, Langmuir isotherm yields a correlation with R^2 value of 0.989 and predicts a maximum adsorption volume (Langmuir volume, V_L) of 0.0548 mmol/g at infinite P_s.

At higher-pressure range, the developed isotherm reveals that Langmuir isotherm is not actually a Type I isotherm but a "*pseudo-Type I*" isotherm.

(Keywords: Type I isotherm, adsorption saturation pressure, Langmuir isotherm, monolayer adsorption)

INTRODUCTION

Adsorption is the adhesion of molecules of a gas, liquid or dissolved solid to a surface to form a thin film of the adsorbate on the adsorbent. Adsorption can be classified as *physisorption* (physical adsorption) or *chemisorption* (chemical adsorption). Practical classification of a particular adsorption as physisorption or chemisorption depends principally on the temperature-dependent binding energy of the adsorbate to the adsorbent. However, the same surface can display physisorption at one temperature and chemisorption at a higher temperature (Moore, 1972).

Gas adsorption (or desorption) occurs when the interaction forces in the region of the phase boundary (i.e., solid surface) is altered. The interaction forces are in the form of: (i) the van der Waals forces that cause physical attraction, (ii) electrostatic/ionic forces that cause surface charge interaction, (iii) covalent bonding that cause chemical attraction, and (iv) the adsorbent hydrophilic or hydrophobic nature.

Three major approaches that form the basis of formulating adsorption models or isotherms are: kinetics, thermodynamics and potential theory (Malek, 1996). Kinetic consideration is based on adsorption equilibrium which is defined as a state of dynamic equilibrium attained when an adsorbate containing phase has been in contact with the adsorbent for sufficient time, with both adsorption and desorption rates being equal (Langmuir, 1916; Ghiaci et al., 2004; Kumar and Sivanesan, 2007).

Different models with various theoretical backgrounds have been applied to describe the adsorption behaviour of fluids. These models include linear adsorption isotherm, Freundlich adsorption isotherm (Freundlich, 1906), Langmuir adsorption isotherm (Langmuir, 1916), extended Langmuir adsorption isotherm (Markham and Benton, 1931), Brunauer-Emmett-Teller (BET) adsorption model (Brunauer et al., 1938), Fowler-Guggenheim adsorption isotherm (Fowler and Guggenheim, 1939), Temkin adsorption isotherm (Temkin and Pyzhev, 1940), Harkins-Jura adsorption isotherm (Harkins and Jura (1943), Langmuir-Freundlich (or Sips) adsorption isotherm (Sips, 1948), Koble–Corrigan adsorption isotherm (Koble and Corrigan, 1952), Kiselev adsorption isotherm (Kiselev, 1958), Redlich-Peterson adsorption isotherm (Redlich and Peterson, 1959),

UNDER PEER REVIEW

Elovich adsorption isotherm (Elovich and. Larinov, 1962), ideal adsorbed solution (IAS) theory (Myers and Prausnitz, 1965), Dubinin's micropores filling models (Dubinin, 1960; Dubinin, 1966; Dubinin and Astakhov, 1971; Dubinin and Radushkevich, 1977), Toth adsorption isotherm (Toth, 1971), multisite occupancy model (Nitta et al., 1984), etc.

The theory-based equilibrium physisorption models applicable to unconventional gas reservoirs are the Ono-Kondo (OK) lattice model, two-dimensional equations of state (2-D EOS) adsorption model (including Hill-de Boer adsorption isotherm), and simplified local density (SLD) models.

The experimentally observed adsorption isotherms are grouped according to IUPAC recommendations in six different types I to VI (**Figure 1**).

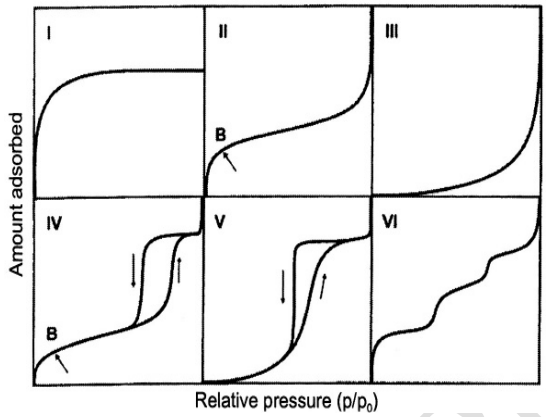

Figure 1: Main types of gas physisorption Isotherms (Source: IUPAC, 1985)

Type I isotherms are characterized by the maximum value the mass adsorbed attains and maintains even at very high gas (or fluid) pressures. The model is applicable in microporous materials exhibiting monolayer adsorption. Type I isotherms are often described by the Langmuir equation. Type II isotherms describe typical adsorption in mesoporous materials exhibiting monolayer at low pressures and multilayer at higher pressures near saturation and pore condensation with no hysteresis. Type II isotherms often can be described by the BET equation (Keller and Staudt, 2005).

Type III isotherms occur in systems where the adsorbate-adsorbate interaction is stronger than the adsorbate-adsorbent interaction. Type IV isotherms describe the adsorption behaviour of special mesoporous materials showing pore condensation together with hysteresis behavior between the adsorption and the desorption paths (Keller and Staudt, 2005).

Type V isotherms (unlike the Type IV isotherms) features nearly perpendicular middle portions of the adsorption and the desorption paths often near relative gas pressures. This shows the existence of mesopores in which phase change like pore condensation may occur. Type VI isotherms is characterized by stepwise multilayer adsorption; the layers becoming more pronounced at low temperatures. (Keller and Staudt, 2005).

Most often, Langmuir isotherm (representing Type I Isotherm) has been used in modelling gas adsorption in coal bed reservoirs, shale gas reservoirs and other monolayer adsorptions cases despite the fact that it yields over-estimation at higher pressures thus contradicting the description of Type I isotherm. Here, higher pressures refer to pressures above the adsorption saturation pressure (P_s). Langmuir isotherm is used in modelling monolayer gas adsorption because of its ease of application and its reliable low-pressure adsorption prediction (Merey, 2013; Adekola *et al*., 2016; Chen *et al*. 2017; Jin *et al*., 2017; Mahatmanti *et al*., 2017; Choy *et al*., 2018; Hamzaoui *et al*., 2018).

Hence, in this work, a new Type-I adsorption isotherm (which assumes a monolayer adsorption like Langmuir isotherm) is developed that discloses and amends this ambiguity.

METHODOLOGY

Physical Depiction of Adsorption in the New Model

The physical depiction of adsorption of the molecules of a fluid F in the new model is shown in **Figure 2** below:

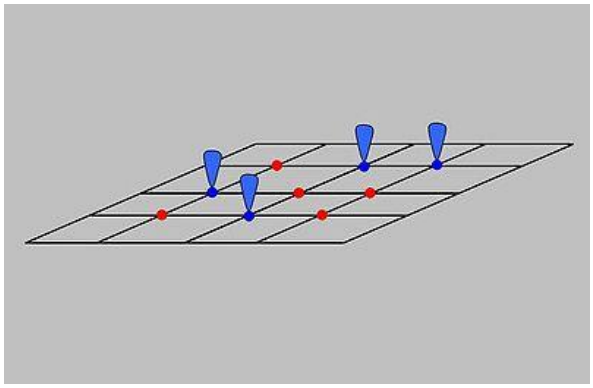

Figure 2: Physical Depiction (Schematic) of Adsorption in the New Model (Source: Langmuir, 1916)

Here, the occupied surface sites are denoted as blue clips while vacant surface sites are denoted as red spots on the surface.

UNDER PEER REVIEW

Assumptions

The basic assumptions made here are similar to those of the Langmuir isotherm. The model assumes an ideal surface where: (i) solid surface is composed of localised adsorption sites, and each site can hold only one adsorbate molecule, (ii) adsorption sites are energetically equivalent i.e. the surface is homogeneous and all sites are identical, (iii) saturation coverage is attained when all sites are completely occupied, (iv) adsorption of molecules is of monolayer type, and (v) adsorption is reversible i.e. desorption occurs during pressure depletion.

Additional (major) assumptions included are: (i) there are adsorbate-adsorbate interactions between neighboring adsorption sites, (ii) attainment of a definite adsorption saturation pressure, and (iii) dynamic equilibrium parameter K_{eq}^{f} is not considered constant (as done in Langmuir isotherm derivation where adsorption coverage is assumed to be independent of the enthalpy of adsorption E) because adsorption coverage actually depends on the enthalpy of adsorption E (adsorption saturation pressure P_s is an index of adsorption coverage).

Development of the New Adsorption Model: Kinetic Approach

In the adsorption of the molecules of a fluid F, the concentration of the occupied surface sites is denoted as $[S_{ads}]$ (number/area) while the vacant surface sites concentration is denoted as $[S_{vac}]$. Total site concentration is $[S_T] = [S_{ads}] + [S_{vac}]$ (number/area)

Rate of adsorption R_{ads} is proportional to the adsorption potential of the fluid (at pressure P) towards saturation coverage of the surface. The saturation coverage is of course attained when all sites $[S_T]$ (number/area) are completely occupied. Attractive interactions causing adsorption are characterized by adsorbates losing activation energy, thus adsorption is an exothermic reaction.

Hence,

$$R_{ads} = \beta_{ads}.P.[S_T] \quad (1)$$

where adsorption rate parameter β_{ads} is expressed as an Arrhenius relation:

$$\beta_{ads} = K_{ads_o} \cdot exp\left(\frac{-E}{RT}\right) \quad (2)$$

and K_{ads_o} is adsorption rate coefficient at the onset of adsorption, E is interaction energy (i.e., heat or enthalpy of adsorption) between the gas molecules and the solid sites, R is universal gas constant and T is temperature.

On the other hand, rate of desorption R_{des} is proportional to the difference between the desorption potential of the fluid (at the adsorption saturation pressure P_s) towards partial coverage of the surface $[S_{ads}]$, and the adsorption potential at a lower pressure P.

$$R_{des} = K_{des} \cdot \{P_s[S_{ads}] - P[S_T]\} \quad (3)$$

where K_{des} is desorption rate coefficient, P_s is the adsorption saturation pressure, the pressure at which adsorbed volume saturation is attained (as pressure increases) and the commencement of gas desorption (during pressure depletion).

The dynamic equilibrium parameter K_{eq}^{f} is expressed as:

$$K_{eq}^{f} = \frac{\beta_{ads}}{K_{des}} = \frac{K_{ads_o}}{K_{des}} \cdot exp\left(\frac{-E}{RT}\right) \quad (4)$$

As stated earlier, K_{eq}^{f} is only constant if adsorption coverage is assumed to be independent of the enthalpy of adsorption E as done in Langmuir isotherm derivation. However, here, K_{eq}^{f} is not considered constant because adsorption coverage actually depends on the enthalpy of adsorption E (adsorption saturation pressure is an index of adsorption coverage).

At dynamic equilibrium, rate of adsorption equals rate of desorption. Hence, the dynamic equilibrium parameter K_{eq}^{f} is expressed as:

$$K_{eq}^{f} = \frac{\beta_{ads}}{K_{des}} = \frac{\{P_s[S_{ads}] - P[S_T]\}}{P[S_T]} \quad (5)$$

$$K_{eq}^{f} = \frac{P_s[S_{ads}]}{P[S_T]} - 1 \quad (6)$$

$$\frac{P_s[S_{ads}]}{P[S_T]} = 1 + K_{eq}^{f} \quad 7)$$

$$\frac{[S_{ads}]}{[S_T]} = \frac{P\left(1+K_{eq}^{f}\right)}{P_s} \quad (8)$$

Expressing the occupied sites $[S_{ads}]$ as the adsorbed volume V at pressure P, and the concentration of all sites $[S_T]$ as the maximum adsorbed volume V_{max} at and above the onset of adsorption saturation pressure i.e. $P \geq P_s$; then

UNDER PEER REVIEW

$$\frac{V}{V_{max}} = \frac{P\left(1+K_{eq}^{f}\right)}{P_s} \quad (9)$$

where K_{eq}^{f} is a measure of the pressure deviation from the corresponding linear isotherm pressure.

$$V = V_{max}\left(\frac{P+K_{eq}^{f}P}{P_s}\right) \quad (10)$$

Expressing $K_{eq}^{f}P$ as P_a the pressure deviation from the corresponding linear isotherm pressure, then

$$V = V_{max}\left(\frac{P}{P_s}+\frac{P_a}{P_s}\right) \quad (11)$$

(1) For under-saturated adsorption, i.e. when $0 \leq P < P_s$

The pressure deviation from the corresponding linear isotherm pressure is proportional to pressure deviation from the adsorption saturated pressure:

$$P_a = k(P_s - P) \quad (12)$$

where k is a dynamic parameter expressed as:

$$k = \left(\frac{P}{P_s}\right)^n \quad (13)$$

and n is adsorbate-adsorbent resistance parameter.

Hence,

$$P_a = (P_s - P)\left(\frac{P}{P_s}\right)^n \quad (14)$$

And K_{eq}^{f} is further simplified as:

$$K_{eq}^{f} = \left(\frac{P}{P_s}\right)^{n-1} - \left(\frac{P}{P_s}\right)^n \quad (15)$$

This shows that the dynamic equilibrium parameter K_{eq}^{f} is a function of pressure P and adsorption saturation pressure P_s: as P changes, K_{eq}^{f} also changes unlike the case in Langmuir isotherm derivation where K_{eq}^{f} is considered constant irrespective of the level of P.

It should be noted that when there is no adsorption, $P = 0$ and thus $P_a = 0$. Also, at the onset of adsorption saturation pressure $P = P_s$ and thus $P_a = 0$.

Substituting **Equation 14** into **Equation 11** gives:

$$V = V_{max}\left\{\frac{P}{P_s}+\left(1-\frac{P}{P_s}\right)\left(\frac{P}{P_s}\right)^n\right\} \quad (16)$$

where V is the adsorbed volume at pressure P, V_{max} is the maximum adsorbed volume at and above the saturation pressure, and n is adsorbate-adsorbent resistance parameter. The major representatives of Type I adsorption isotherm pressure-volume data (below the adsorption saturation pressure) are captured and depicted by the adsorbate-adsorbent resistance parameter n ranging from 0.30 to 1.15.

(2) For saturated adsorption, i.e. when $P \geq P_s$

The adsorption saturated pressure P_s is the effective pressure while additional increase in pressure is latent; hence, the heat of adsorption $E = 0$. Thus

$$V = V_{max} \quad (17)$$

Statement of the Developed Adsorption Isotherm

The developed adsorption isotherm is stated as follows:

$$V = \begin{Bmatrix} V_{max}\left\{\frac{P}{P_s}+\left(1-\frac{P}{P_s}\right)\left(\frac{P}{P_s}\right)^n\right\}, for\ P < P_s \\ V_{max},\ for\ P \geq P_s \end{Bmatrix} \quad (18)$$

where V is the adsorbed volume at equilibrium pressure P, P_s is the adsorption saturation pressure at which the maximum adsorbed volume V_{max} is attained, n is adsorbate-adsorbent resistance parameter (n ranges from 0.30 to 1.15).

Establishment of Boundary Conditions for the Developed Adsorption Isotherm

The graphical analysis of establishing boundary conditions for the developed adsorption isotherm is shown in **Figure 3**.

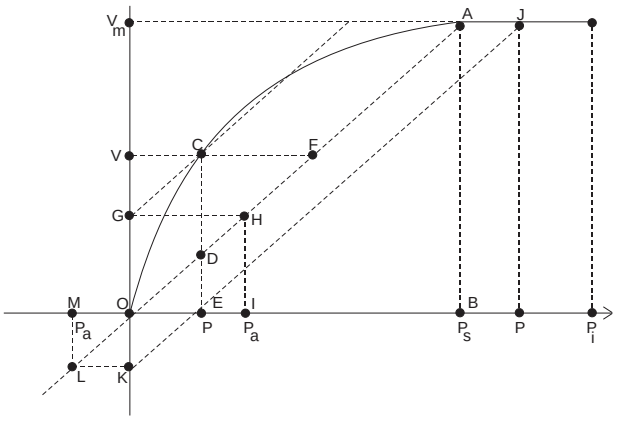

Figure 3: Graphical analysis of the developed adsorption isotherm

For an adsorbed volume V, point C on the isotherm is projected downwards to meet line $\overline{OA}$ at D and the pressure axis at E. The volume deviation from

UNDER PEER REVIEW

the corresponding linear isotherm volume is $\overline{CD} = \delta$.

Along $\overline{OA}$,

$$slope = \frac{\overline{DE}}{\overline{OE}} = \frac{\overline{AB}}{\overline{OB}} \quad (19)$$

but

$$\overline{DE} = \overline{CE} - \overline{CD} \quad (20)$$

i.e.

$$\overline{DE} = V - \delta \quad (21)$$

Hence,

$$slope = \frac{V-\delta}{P} = \frac{V_{max}}{P_s} \quad (22)$$

$$\frac{V-\delta}{V_{max}} = \frac{P}{P_s} \quad (23)$$

$$\frac{V}{V_{max}} = \frac{P}{P_s} + \frac{\delta}{V_{max}} \quad (24)$$

Point C on the isotherm is again projected horizontally to meet $\overline{OA}$ at F. Also, at C a line of equal slope as $\overline{OA}$ is projected to intercept the volume axis at G, and meet $\overline{OA}$ and the pressure axis at H and I respectively. The pressure deviation from the corresponding linear isotherm pressure is $\overline{CF} = P_a$.

$$P_a = \overline{CF} = \overline{GH} = \overline{OI} \quad (25)$$

Also,

$$\delta = \overline{CD} = \overline{GO} = \overline{HI} \quad (26)$$

Along $\overline{OA}$,

$$slope = \frac{\overline{HI}}{\overline{OI}} = \frac{\overline{AB}}{\overline{OB}} \quad (27)$$

$$\frac{\delta}{P_a} = \frac{V_{max}}{P_s} \quad (28)$$

$$\frac{\delta}{V_{max}} = \frac{P_a}{P_s} \quad (29)$$

Substituting **Equation 29** into **Equation 24** gives:

$$\frac{V}{V_{max}} = \frac{P}{P_s} + \frac{P_a}{P_s} \quad (30)$$

i.e.

$$V = V_{max}\left(\frac{P+P_a}{P_s}\right) \quad (31)$$

Establishment of Boundary Conditions for P_a

Boundary conditions for P_a, the pressure deviation from the corresponding linear isotherm, is highlighted thus:

1. $P_a = 0$ at $P = 0$ and $P = P_s$
2. $P_a > 0$ within the pressure range $0 < P < P_s$
3. P_a is maximum $(\frac{dP_a}{dP} = 0)$ i.e. $\frac{d}{dP}\{(P_s - PPPsn{=}0$ at the inflexion point β of the isotherm within the pressure range $0 < P < P_s$. At the inflexion point β, $\Delta\left(\frac{V}{V_{max}}\right) = \Delta\left(\frac{P}{P_s}\right)$.
4. For saturated adsorption, i.e. when $P > P_s$, at J (see **Figure 3**), a line of equal slope as $\overline{OA}$ is projected to intercept the volume axis at K and meet $\overline{OA}$ extension and the pressure axis at L and M respectively.

$$P_a = \overline{OM} = \overline{KL} = -\overline{AJ} \quad (32)$$

$$P_a = -(P - P_s) \quad (33)$$

$$P_a = P_s - P \quad (34)$$

and

$$V = V_{max} \quad (35)$$

Plot of Relative Adsorbed Volume versus Relative Pressure for the Developed Adsorption Isotherm

For pressure range below adsorption saturation pressure $(P < P_s)$, the developed adsorption isotherm $\frac{V}{V_{max}} = \left\{\frac{P}{P_s} + \left(1 - \frac{P}{P_s}\right)\left(\frac{P}{P_s}\right)^n\right\}$ could be expressed as:

$$Y = \{X + (1 - X)(X)^n\} \quad (36)$$

A plot of Y versus X is shown in **Figure 4**. As stated earlier, the major representatives of Type I adsorption isotherm pressure-volume data (below the adsorption saturation pressure) are captured and depicted by the adsorbate-adsorbent resistance parameter n ranging from 0.30 to 1.15.

UNDER PEER REVIEW

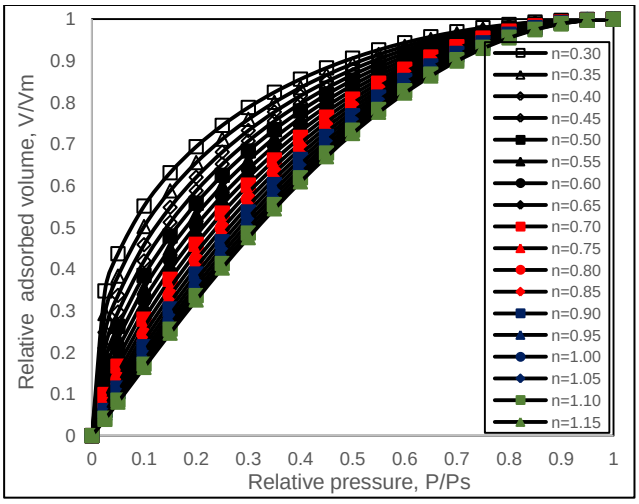

Figure 4: Plot of relative adsorbed volume versus relative pressure for the developed adsorption isotherm

Parameterisation of Experimental Adsorption Data using the Developed Isotherm

The steps involved in the developed isotherm parameters evaluation from experimental data are as highlighted below:

1. Produce the experimental adsorption isotherm by plotting the adsorbed volume V versus pressure P.
2. Compare and match the experimental isotherm with the relative adsorbed volume–relative pressure curve (see **Figure 4**) and select a few adsorbate-adsorbent resistance parameter n of closer range.
3. For each n selected, feature the corresponding parameters $b = \frac{V_{last}}{V_{max}}$ and $c = \frac{P_{last}}{P_s}$ (see **Tables 1, 2** and **3**) where P_{last}, V_{last} are the last P,V values of the experimental adsorption data. Thus evaluate the corresponding $V_{max} = \frac{V_{last}}{b}$ and $P_s = \frac{P_{last}}{c}$, and the pressure P_β, and adsorbed volume V_β at the inflexion point β where $\Delta\left(\frac{V}{V_{max}}\right) = \Delta\left(\frac{P}{P_s}\right)$ on the developed isotherm (see **Table 4**). Note that $\frac{V_{last}}{V_{max}} = \left\{\frac{P_{last}}{P_s} + \left(1 - \frac{P_{last}}{P_s}\right)\left(\frac{P_{last}}{P_s}\right)^n\right\}$.

Table 1: Table of adsorption saturation data for establishing the boundary conditions of the developed isotherm ($n = 0.30$ *to* 0.55)

$b = \frac{V_{last}}{V_{max}}$	$n = 0.30$	$n = 0.35$	$n = 0.40$	$n = 0.45$	$n = 0.50$	$n = 0.55$
	$c = \frac{P_{last}}{P_s}$	$c = \frac{P_{last}}{P_s}$	$c = \frac{P_{last}}{P_s}$	$c = \frac{P_{last}}{P_s}$	$c = \frac{P_{last}}{P_s}$	$c = \frac{P_{last}}{P_s}$
0.920	0.5339	0.5621	0.5853	0.6049	0.6218	0.6365
0.925	0.5470	0.5746	0.5974	0.6166	0.6331	0.6474
0.930	0.5607	0.5877	0.6100	0.6287	0.6448	0.6588
0.935	0.5751	0.6014	0.6231	0.6413	0.6570	0.6706
0.940	0.5901	0.6157	0.6368	0.6545	0.6697	0.6830
0.945	0.6060	0.6308	0.6512	0.6684	0.6831	0.6959
0.950	0.6227	0.6467	0.6664	0.6830	0.6972	0.7095
0.955	0.6405	0.6636	0.6825	0.6984	0.7120	0.7238
0.960	0.6594	0.6815	0.6996	0.7148	0.7278	0.7390
0.965	0.6799	0.7009	0.7180	0.7324	0.7447	0.7553
0.970	0.7021	0.7218	0.7380	0.7514	0.7629	0.7730
0.975	0.7265	0.7449	0.7598	0.7723	0.7830	0.7922
0.980	0.7539	0.7706	0.7842	0.7956	0.8052	0.8136
0.985	0.7855	0.8002	0.8122	0.8222	0.8307	0.8381
0.990	0.8235	0.8358	0.8458	0.8541	0.8612	0.8673
0.995	0.8739	0.8829	0.8902	0.8962	0.9013	0.9057
1.000	1.0000	1.0000	1.0000	1.0000	1.0000	1.0000

Table 2: Table of adsorption saturation data for establishing the boundary conditions of the developed isotherm ($n = 0.60$ *to* 0.85)

$b = \frac{V_{last}}{V_{max}}$	$n = 0.60$	$n = 0.65$	$n = 0.70$	$n = 0.75$	$n = 0.80$	$n = 0.85$
	$c = \frac{P_{last}}{P_s}$	$c = \frac{P_{last}}{P_s}$	$c = \frac{P_{last}}{P_s}$	$c = \frac{P_{last}}{P_s}$	$c = \frac{P_{last}}{P_s}$	$c = \frac{P_{last}}{P_s}$
0.920	0.6495	0.6610	0.6714	0.6808	0.6893	0.6972
0.925	0.6601	0.6714	0.6815	0.6907	0.6990	0.7066
0.930	0.6711	0.6821	0.6920	0.7009	0.7090	0.7165
0.935	0.6826	0.6933	0.7029	0.7116	0.7194	0.7266
0.940	0.6946	0.7050	0.7142	0.7226	0.7303	0.7372
0.945	0.7071	0.7171	0.7261	0.7342	0.7416	0.7483

UNDER PEER REVIEW

0.950	0.7203	0.7299	0.7385	0.7463	0.7534	0.7599
0.955	0.7342	0.7434	0.7517	0.7591	0.7659	0.7721
0.960	0.7489	0.7577	0.7656	0.7727	0.7791	0.7850
0.965	0.7647	0.7730	0.7804	0.7871	0.7932	0.7988
0.970	0.7817	0.7895	0.7964	0.8027	0.8084	0.8136
0.975	0.8003	0.8075	0.8139	0.8197	0.8249	0.8297
0.980	0.8210	0.8274	0.8333	0.8385	0.8432	0.8476
0.985	0.8445	0.8502	0.8553	0.8599	0.8641	0.8679
0.990	0.8727	0.8774	0.8816	0.8854	0.8889	0.8920
0.995	0.9096	0.9130	0.9161	0.9188	0.9213	0.9236
1.000	1.0000	1.0000	1.0000	1.0000	1.0000	1.0000

Table 3: Table of adsorption saturation data for establishing the boundary conditions of the developed isotherm ($n = 0.90$ *to* 1.15)

$b = \frac{V_{last}}{V_{max}}$	$n = 0.90$	$n = 0.95$	$n = 1.00$	$n = 1.05$	$n = 1.10$	$n = 1.15$
	$c = \frac{P_{last}}{P_s}$	$c = \frac{P_{last}}{P_s}$	$c = \frac{P_{last}}{P_s}$	$c = \frac{P_{last}}{P_s}$	$c = \frac{P_{last}}{P_s}$	$c = \frac{P_{last}}{P_s}$
0.920	0.7044	0.7110	0.7172	0.7230	0.7283	0.7334
0.925	0.7136	0.7202	0.7262	0.7318	0.7370	0.7420
0.930	0.7233	0.7296	0.7355	0.7409	0.7460	0.7508
0.935	0.7333	0.7394	0.7451	0.7504	0.7553	0.7600
0.940	0.7437	0.7496	0.7551	0.7602	0.7650	0.7695
0.945	0.7545	0.7602	0.7665	0.7705	0.7751	0.7794
0.950	0.7658	0.7713	0.7764	0.7812	0.7856	0.7898
0.955	0.7778	0.7830	0.7879	0.7925	0.7967	0.8006
0.960	0.7904	0.7954	0.8000	0.8044	0.8084	0.8121
0.965	0.8039	0.8086	0.8130	0.8170	0.8208	0.8244
0.970	0.8184	0.8228	0.8268	0.8306	0.8342	0.8375
0.975	0.8341	0.8382	0.8419	0.8454	0.8487	0.8517
0.980	0.8516	0.8552	0.8586	0.8618	0.8647	0.8675
0.985	0.8714	0.8746	0.8776	0.8803	0.8829	0.8853
0.990	0.8949	0.8976	0.9000	0.9023	0.9045	0.9065
0.995	0.9257	0.9276	0.9293	0.9310	0.9325	0.9339
1.000	1.0000	1.0000	1.0000	1.0000	1.0000	1.0000

Table 4: Table of P-V parameters at point β where $\Delta\left(\frac{V}{V_{max}}\right) = \Delta\left(\frac{P}{P_s}\right)$

	$n = 0.30$	$n = 0.35$	$n = 0.40$	$n = 0.45$	$n = 0.50$	$n = 0.55$
$P_\beta = \frac{n}{n+1}P_s$	$\frac{3}{13}P_s$	$\frac{7}{27}P_s$	$\frac{2}{7}P_s$	$\frac{9}{29}P_s$	$\frac{1}{3}P_s$	$\frac{11}{31}P_s$
V_β	$0.7262V_{max}$	$0.7211V_{max}$	$0.7185V_{max}$	$0.7177V_{max}$	$0.7182V_{max}$	$0.7197V_{max}$
	$n = 0.60$	$n = 0.65$	$n = 0.70$	$n = 0.75$	$n = 0.80$	$n = 0.85$
$P_\beta = \frac{n}{n+1}P_s$	$\frac{3}{8}P_s$	$\frac{13}{33}P_s$	$\frac{7}{17}P_s$	$\frac{3}{7}P_s$	$\frac{4}{9}P_s$	$\frac{17}{37}P_s$
V_β	$0.7220V_{max}$	$0.7247V_{max}$	$0.7278V_{max}$	$0.7312V_{max}$	$0.7348V_{max}$	$0.7385V_{max}$
	$n = 0.90$	$n = 0.95$	$n = 1.00$	$n = 1.05$	$n = 1.10$	$n = 1.15$
$P_\beta = \frac{n}{n+1}P_s$	$\frac{9}{19}P_s$	$\frac{19}{39}P_s$	$\frac{1}{2}P_s$	$\frac{21}{41}P_s$	$\frac{11}{21}P_s$	$\frac{23}{43}P_s$
V_β	$0.7423V_{max}$	$0.7462V_{max}$	$0.7500V_{max}$	$0.7538V_{max}$	$0.7576V_{max}$	$0.7614V_{max}$

The details of the evaluation of pressure P_β and adsorbed volume V_β at point β where $\Delta\left(\frac{V}{V_{max}}\right) = \Delta\left(\frac{P}{P_s}\right)$ on the developed isotherm are shown in **Appendix B.**

4. Choose the P_β, V_β values that correlate with the experimental adsorption isotherm, and thus consider the corresponding n, P_s and V_{max} as the parameters of the developed adsorption isotherm for the experimental adsorption data.
5. Model the experimental adsorption data as:

$$V = \begin{Bmatrix} V_{max}\left\{\frac{P}{P_s} + \left(1 - \frac{P}{P_s}\right)\left(\frac{P}{P_s}\right)^n\right\}, for\ P < P_s \\ V_{max},\ for\ P \geq P_s \end{Bmatrix} \quad (37)$$

where V is the adsorbed volume at equilibrium pressure P, P_s is the adsorption saturation pressure at which the maximum adsorbed volume V_{max} is attained, n is adsorbate-adsorbent resistance parameter (n ranges from 0.30 to 1.15).

UNDER PEER REVIEW

Parameterisation of Experimental Adsorption Data Using Langmuir Isotherm

The steps involved in Langmuir isotherm parameters evaluation from experimental data are as highlighted below:

1. Obtain the parameters V_L and P_L (Langmuir volume and Langmuir pressure respectively) by arranging the isotherm $V = V_L\left(\frac{P}{P+P_L}\right)$ thus:

$$\frac{P}{V} = \left(\frac{1}{V_L}\right)P + \left(\frac{1}{V_L}\right)P_L \quad (38)$$

2. Plot $\frac{P}{V}$ versus P to yield the equation of a straight line: $Y = mX + C$, where slope $m = \frac{1}{V_L}$ and Y-axis intercept $C = \left(\frac{1}{V_L}\right)P_L$ are obtained from the best fit line.

3. Model the laboratory adsorption data using the two parameters V_L and P_L as:

$$V = V_L\frac{P}{P+P_L} \quad (39)$$

Generalisation of the Developed Isotherm

The step involved are as follows:

1. Plot V versus P for the experimental data, the proposed isotherm and Langmuir isotherm.
2. Correlate the developed isotherm with Langmuir isotherm and validate with the experimental data using statistical deviation (error) parameters.

Statement of Developed Isotherm for Gas Mixture

With reference to the pure-component adsorption isotherm developed in this study, the volume of the adsorbing specie i in a mixture of gases at an equilibrium pressure P is expressed:

$$V_i = \left(\frac{y_i(V_{max})_i}{\sum_{j=1}^{N} y_j(V_{max})_j}\right) * (V_{100\%})_i \quad (40)$$

where y_i is the gas-phase mole fraction (or the feed ratio) of the adsorbing specie i; $(V_{max})_i$ is the maximum adsorbed volume of the adsorbing specie i of 100% concentration; y_j is the gas-phase mole fraction (or the feed ratio) of the respective specie j; $(V_{max})_j$ is maximum adsorbed volume of the respective specie j of 100% concentration; $j = 1, \ldots . N$; N is the number of gas specie; $(V_{100\%})_i$ is the volume of the adsorbing specie i of 100% concentration at the corresponding pressure.

Correlation of the Developed Isotherm for Gas Mixture with the Extended Langmuir Isotherm

The mixing rule for the developed adsorption isotherm (for gas mixture) is correlated with the extended Langmuir isotherm expressed as:

$$V_i = (V_L)_i\frac{y_i b_i P}{\left(1+\sum_{j=1}^{N} y_j b_j P\right)} \quad (41)$$

where y_i is the gas-phase mole fraction of the adsorbing specie i; b_i is equal to $1/P_{L_i}$, the temperature-dependent pure-component Langmuir model parameter;; P is equilibrium pressure; and $j = 1, \ldots . N$; N is the number of gas component.

Statistical Deviation (Error) Parameters Used

The statistical deviation (error) parameters used in assessing the quality of fit in the adsorption model representation are the weighted root mean square (WRMS) deviation, the weighted average absolute deviation (WAAD), the percent average absolute deviation (%AAD) and the root mean square error (RMSE). These parameters are expressed as follows:

$$WRMS = \sqrt{\frac{1}{N}\cdot\sum_{i=1}^{N}\left(\frac{V_{cal}-V_{exp}}{\sigma_{exp}}\right)_i^2} \quad (42)$$

$$WAAD = \frac{1}{N}\cdot\sum_{i=1}^{N} abs\left(\frac{V_{cal}-V_{exp}}{\sigma_{exp}}\right)_i \quad (43)$$

$$\%AAD = \frac{1}{N}\cdot\sum_{i=1}^{N} abs\left(\frac{V_{cal}-V_{exp}}{V_{exp}}\right)_i \times 100\% \quad (44)$$

and

$$RMSE = \sqrt{\frac{1}{N}\cdot\sum_{i=1}^{N}\left(V_{cal}-V_{exp}\right)_i^2} \quad (45)$$

Here, i is the data point, N is the number of data points, V_{exp} is the experimental adsorption volume, V_{cal} is the calculated adsorption volume and σ_{exp} is the expected experimental uncertainty.

RESULTS AND DISCUSSION

Experimental Pure Gas Adsorption Data Employed

The developed isotherm can be used to model all cases of monolayer adsorptions of gases (or fluids) on adsorbents. However, in this research work, experimental pure gas adsorption data employed are highlighted in **Tables 5, 6** and **7** where the absolute uncertainty in adsorption is denoted as σ_{Exp}:

Table 5: Pure methane adsorption on Turkey's shale sample at 25 ^{o}C (i.e. 77 ^{o}F)

Pressure, P (psia)	Gibbs adsorption, V (mmol/g)	σ_{Exp} (mmol/g)
190	0.0197	0.0024
403	0.0265	0.0037
602	0.0325	0.0050
805	0.0361	0.0063
1002	0.0394	0.0077

UNDER PEER REVIEW

1201	0.0412	0.0092
1403	0.0437	0.0107
1598	0.0446	0.0122
1798	0.0447	0.0137
2005	0.0450	0.0153

(Source: Merey, 2013)

Table 6: Pure methane adsorption on dryTiffany mixed coal sample at 130 ^{o}F

Pressure, P (psia)	**Absolute adsorption, V (scf/ton)**	**σ_{Exp} (scf/ton)**
255.9	117.0	3.510
824.9	243.9	7.317
1210.2	283.6	8.508
1796.9	316.6	9.498

(Source: Gasem *et al*., 2002)

Note: σ_{Exp} were evaluated based on average expected experimental uncertainty of 3%

Table 7: Pure nitrogen adsorption on dry Tiffany mixed coal sample at 130 ^{o}F

Pressure, P (psia)	**Absolute adsorption, V (scf/ton)**	**σ_{Exp} (scf/ton)**
106.6	18.1	1.086
202.9	29.9	1.794
406.0	52.9	3.174
602.7	69.7	4.182
795.6	88.1	5.286
1000.2	102.3	6.138
1202.5	113.9	6.834
1410.9	126.6	7.596
1604.9	138.0	8.280
1806.2	147.2	8.832

(Source: Gasem *et al*., 2002)

Note: σ_{Exp} were evaluated based on average expected experimental uncertainty of 6%

Methane Adsorption on Turkey's Shale Sample at 25 ^{o}C (Source: Merey, 2013)

Parameterisation of Methane Adsorption on Turkey's Shale Sample at 25 ^{o}C using the Developed Isotherm

Plotting the experimental isotherm from **Table 5** and matching it with the relative adsorbed volume – relative pressure curve (see **Figure 4**) shows n to be in the range of 0.35 to 0.45. For each n, the corresponding parameters $b = \frac{V_{last}}{V_{max}}$ and $c = \frac{P_{last}}{P_s}$ were featured. Using ***Excel*** spreadsheet programming; the corresponding $V_{max} = \frac{V_{last}}{b}$ and $P_s = \frac{P_{last}}{c}$, and the pressure and adsorbed volume at the inflexion point β where $\Delta\left(\frac{V}{V_{max}}\right) = \Delta\left(\frac{P}{P_s}\right)$ on the isotherms were evaluated. The adsorption resistance parameter $n = 0.40$ yields the P_β, V_β values that correlate with the experimental adsorption isotherm as shown in **Table 8** below:

Table 8: Adsorption saturation data for establishing the boundary conditions of the developed isotherm for methane adsorption on Turkey's shale sample at 25 ^{o}C (Here, $V_{last} = 0.0450\ mmol/g$ and $P_{last} = 2005\ psia$).

$b = \frac{V_{last}}{V_{max}}$	$n = 0.40$				
	$c = \frac{P_{last}}{P_s}$	$V_{max} = \frac{V_{last}}{b}$ (mmol/g)	$P_s = \frac{P_{last}}{c}$ (psia)	$V_\beta = 0.7185 V_{max}$ (mmol/g)	$P_\beta = \frac{2}{7} P_s$ (psia)
0.955	0.6825	0.0471	2938	0.0338	839
0.960	0.6996	0.0469	2866	0.0337	819
0.965	0.7180	0.0466	2793	0.0335	798
0.970	0.7380	0.0464	2717	0.0333	776
0.975	0.7598	0.0461	2639	0.0331	754
0.980	0.7842	0.0459	2557	0.0330	731
0.985	0.8122	0.0457	2469	0.0328	705
0.990	0.8458	0.0454	23721	0.0326	677
0.995	0.8902	0.0452	2252	0.0325	643
1.000	1.000	**0.0450**	**2005**	**0.0323**	**572**

The P_β, V_β values of **572 psia** and **0.0323 mmol/g** correlate with the experimental isotherm (see **Figure 5**), and the corresponding P_s, V_{max} values **2005 psia** and **0.0450 mmol/g** are considered as the developed isotherm parameters for the experimental adsorption data.

UNDER PEER REVIEW

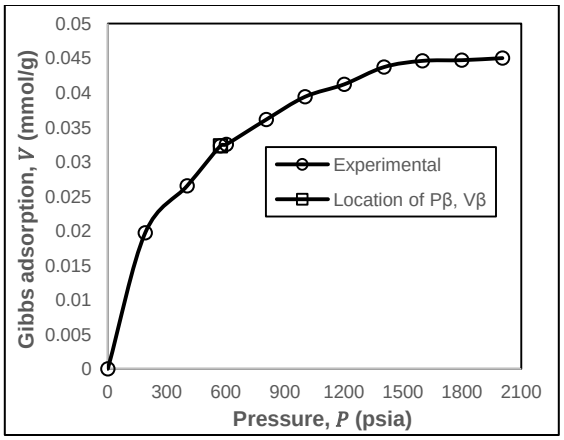

Figure 5: Location of P_β, V_β correlation on the experimental isotherm for methane adsorption on Turkey's shale sample B at 25 ^oC

Hence, methane adsorption on Turkey's shale sample at 25 ^oC is modelled as:

$$V\ (mmol/g) = \left\{ 0.0450 \left\{ \frac{P}{2005} + \left(1 - \frac{P}{2005}\right) \frac{P}{2005}^{0.40} \right\}, P < 2005\ psia \right\} \\ \left\{ 0.0450\ , P \geq 2005\ psia \right\} \quad (46)$$

where maximum adsorbed volume $V_{max} = 0.0450\ mmol/g$, adsorption saturation pressure $P_s = 2005\ psia$, and $n = 0.40$ is a parameter that defines the Turkey's shale sample resistance to methane at 25 ^oC.

Prediction of Methane Adsorption on Turkey's Shale Sample at 25 ^oC using the Developed Isotherm

Prediction of methane adsorption on Turkey's shale sample at 25 ^oC using the developed isotherm, and the corresponding deviation/error analysis parameters are presented in **Table 9** below:

Table 9 Prediction of methane adsorption on Turkey's shale sample at 25 ^oC using the developed isotherm

Pressure, P (psia)	Gibbs adsorption, V (mmol/g)		Deviation (Error) Analysis			
	Experimental	Developed Isotherm	σ_{Exp} (mmol/g)	$V_{Cal} - V_{Exp}$ (mmol/g)	$\frac{V_{Cal} - V_{Exp}}{\sigma_{Exp}}$	$\frac{V_{Cal} - V_{Exp}}{V_{Exp}}$
190	0.0197	0.0201	0.0024	0.0004	0.1667	0.0203
403	0.0265	0.0280	0.0037	0.0015	0.4054	0.0566
602	0.0325	0.0330	0.0050	0.0005	0.1000	0.0154
805	0.0361	0.0368	0.0063	0.0007	0.1111	0.0194
1002	0.0394	0.0395	0.0077	0.0001	0.0130	0.0025
1201	0.0412	0.0417	0.0092	0.0005	0.0543	0.0121
1403	0.0437	0.0432	0.0107	-0.0005	-0.0467	-0.0114
1598	0.0446	0.0442	0.0122	-0.0004	-0.0330	-0.0090
1798	0.0447	0.0448	0.0137	0.0001	0.0073	0.0022
2005	0.0450	0.0450	0.0153	0	0	0

Here, weighted root mean square, WRMS = 0.1486, weighted average absolute deviation, WAAD = 0.0937, percent average absolute deviation, %AAD = 1.4890, root mean square error, RMSE = 0.0006 mmol/g and R^2 value = 0.9973.

Parameterisation of Methane Adsorption on Turkey's Shale Sample at 25 ^oC using Langmuir Isotherm

The variations of $^P/_V$ versus P for methane adsorption on Turkey's shale sample at 25 ^oC is shown in **Table 10**.

Table 10: Parameters for plotting Langmuir isotherm for methane adsorption on Turkey's shale sample at 25 ^oC

Experimental		$\frac{Pressure}{Volume}$, $^P/_V$
Pressure, P (psia)	Gibbs adsorption, V (mmol/g)	(psia/mmol/g)
190	0.0197	9645
403	0.0265	15207
602	0.0325	18523
805	0.0361	22230
1002	0.0394	25431
1201	0.0412	29150
1403	0.0437	32105
1598	0.0446	34739
1798	0.0447	40224
2005	0.0450	44556

The best fit line of the plot of $^P/_V$ versus P (shown in **Figure 6**) yields the equation: $Y = 18.261x + 7081.4$ with R^2 of 0.9952, where slope $m = 18.261 = {}^1/_{V_L}$ and Y-axis intercept $C = 7081.4 = \frac{1}{V_L} P_L$.

UNDER PEER REVIEW

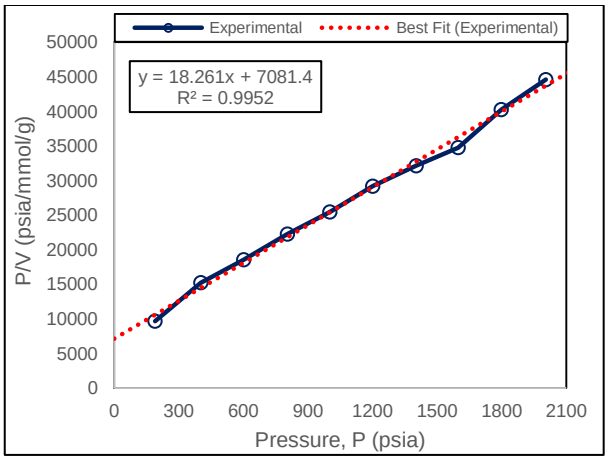

Figure 6: Plot of $\frac{P}{V}$ versus P for methane adsorption on Turkey's shale sample at 25 ^{o}C

Here, Langmuir volume $\boldsymbol{V_L}$ and Langmuir pressure $\boldsymbol{P_L}$ are respectively obtained as **0.0548 mmol/g** and **387.79 psia**. Hence, methane adsorption on Turkey's shale sample at 25 ^{o}C is modelled as:

$$V = 0.0548 * \frac{P}{P+387.79} \qquad mmol/g \qquad (47)$$

where Langmuir constant $b = \frac{1}{P_L} = 0.002579\ psia^{-1}$

Prediction of Methane Adsorption on Turkey's Shale Sample at 25 ^{o}C using Langmuir Isotherm

Prediction of methane adsorption on Turkey's shale sample at 25 ^{o}C using Langmuir isotherm, and the corresponding deviation/error analysis parameters are presented in **Table 11** below.

Table 11: Prediction of methane adsorption on Turkey's shale sample at 25 ^{o}C using Langmuir isotherm

Pressure, P (psia)	Gibbs adsorption, V (mmol/g)		Deviation (Error) Analysis			
	Experimental	Langmuir Isotherm	σ_{Exp} (mmol/g)	$V_{Cal} - V_{Exp}$ (mmol/g)	$\frac{V_{Cal} - V_{Exp}}{\sigma_{Exp}}$	$\frac{V_{Cal} - V_{Exp}}{V_{Exp}}$
190	0.0197	0.0180	0.0024	-0.0017	-0.7083	-0.0863
403	0.0265	0.0279	0.0037	0.0014	0.3784	0.0528
602	0.0325	0.0333	0.0050	0.0008	0.1600	0.0246
805	0.0361	0.0370	0.0063	0.0009	0.1429	0.0249
1002	0.0394	0.0395	0.0077	0.0001	0.0130	0.0025
1201	0.0412	0.0414	0.0092	0.0002	0.0217	0.0049
1403	0.0437	0.0429	0.0107	-0.0008	-0.0748	-0.0183
1598	0.0446	0.0441	0.0122	-0.0005	-0.0410	-0.0112
1798	0.0447	0.0451	0.0137	0.0004	0.0292	0.0089
2005	0.0450	0.0459	0.0153	0.0009	0.0588	0.0200

Here, weighted root mean square, WRMS = 0.2652, weighted average absolute deviation, WAAD = 0.1628, percent average absolute deviation, %AAD = 2.5440, root mean square error, RMSE = 0.0009 mmol/g and R^2 value = 0.9891.

Generalisation of the Developed Isotherm for Methane Adsorption on Turkey's Shale Sample at 25 ^{o}C

To validate and generalise the developed isotherm, predictions of methane adsorption on Turkey's shale sample at 25 ^{o}C by Langmuir and the developed isotherms are correlated with the experimental data as shown in **Table 12** and **Figure 7** below.

Table 12: Generalisation of the developed isotherm for methane adsorption on Turkey's shale sample at 25 ^{o}C

Pressure, P (psia)	Gibbs adsorption, V (mmol/g)		
	Experimental	Developed Isotherm	Langmuir Isotherm
190	0.0197	0.0201	0.0180
403	0.0265	0.0280	0.0279
602	0.0325	0.0330	0.0333
805	0.0361	0.0368	0.0370
1002	0.0394	0.0395	0.0395
1201	0.0412	0.0417	0.0414
1403	0.0437	0.0432	0.0429
1598	0.0446	0.0442	0.0441
1798	0.0447	0.0448	0.0451
2005	0.0450	0.0450	0.0459

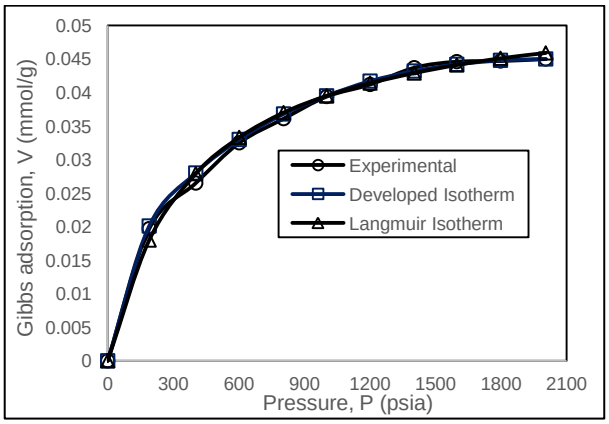

Figure 7: Generalisation of the developed isotherm for methane adsorption on Turkey's shale sample at 25 ^{o}C

UNDER PEER REVIEW

Comparison of High Pressure Adsorption Predictions for Methane Adsorption on Turkey's Shale Sample at 25 ^{o}C

Langmuir and the developed isotherms predictions of methane adsorption on Turkey's shale sample at 25 ^{o}C for high-pressure range are compared in **Table 13** and **Figure 8** below.

Table13: Langmuir and the developed predictions of methane adsorption on Turkey's shale sample at 25 ^{o}C for high-pressure range

Pressure, P (psia)	Gibbs adsorption, V (mmol/g)	
	Developed Isotherm	Langmuir Isotherm
190	0.0201	0.0180
602	0.0330	0.0333
1002	0.0395	0.0395
1403	0.0432	0.0429
1798	0.0448	0.0451
2005	0.0450	0.0459
2400	0.0450	0.0472
2800	0.0450	0.0481
3200	0.0450	0.0489
3600	0.0450	0.0495
4000	0.0450	0.0500

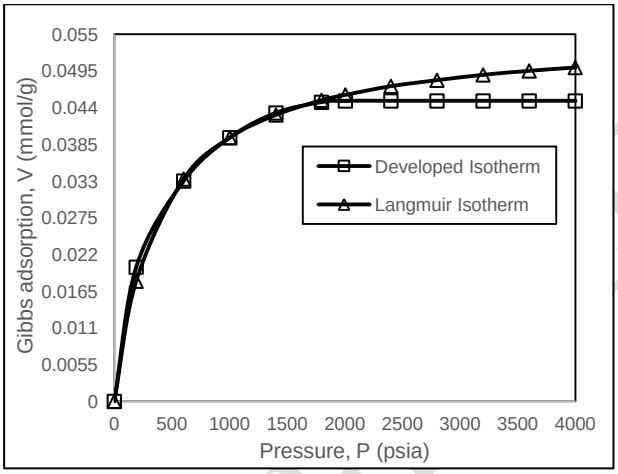

Figure 8: Predictions of methane adsorption on Turkey's shale sample at 25 ^{o}C for high-pressure range by the developed and Langmuir isotherms

The developed isotherm predicts a maximum adsorption volume of **0.0450 mmol/g** at an adsorption saturated pressure of **2005 psia**. However, by Langmuir isotherm prediction, a maximum adsorption volume of **0.0548 mmol/g** is attained at an infinite adsorption saturated pressure. **Figure 7** shows that adsorption prediction by Langmuir isotherm is not reliable at higher pressures because of its inefficiency in defining the onset of adsorption saturation pressure; this contributes to an overestimation of maximum adsorbed volume.

Methane Adsorption on Tiffany Mixed Coal Sample at 130 ^{O}F (Source: Gasem *et al*., 2002)

Parameterisation of Methane Adsorption on Tiffany Mixed Coal Sample at 130 ^{O}F

Plotting the experimental isotherm from **Table 6** and matching it with the relative adsorbed volume – relative pressure curve (see **Figure 4**) shows n to be in the range of 0.45 to 0.55. For each n, the corresponding parameters $b = \frac{V_{last}}{V_{max}}$ and $c = \frac{P_{last}}{P_s}$ were featured. Using ***Excel*** spreadsheet programming; the corresponding $V_{max} = \frac{V_{last}}{b}$ and $P_s = \frac{P_{last}}{c}$, and the pressure and adsorbed volume at the inflexion point β where $\Delta\left(\frac{V}{V_{max}}\right) = \Delta\left(\frac{P}{P_s}\right)$ on the isotherms were evaluated. The adsorption resistance parameter $n = 0.40$ yields the P_β, V_β values that correlate with the experimental adsorption isotherm as shown in **Table 14** below.

Table 14: Adsorption saturation data for establishing the boundary conditions of the developed isotherm for pure methane adsorption on dry Tiffany mixed coal sample at 130 ^{o}F (Here, V_{last} = 316.6 scf/ton and P_{last} = 1,796.9 psia)

$b = \frac{V_{last}}{V_{max}}$	n =0.50				
	$c = \frac{P_{last}}{P_s}$	$V_{max} = \frac{V_{last}}{b}$ (scf/ton)	$P_s = \frac{P_{last}}{c}$ (psia)	$V_\beta = 0.7182 V_{max}$ (scf/ton)	$P_\beta = \frac{1}{3}P_s$ (psia)
0.955	0.7120	331.5	2523.7	238.1	841.2
0.960	0.7278	329.8	2468.9	236.9	823.0
0.965	0.7447	328.1	2412.9	235.6	804.3
0.970	0.7629	326.4	2355.3	234.4	785.1
0.975	0.7830	**324.7**	**2294.9**	**233.2**	**765.0**
0.980	0.8052	323.1	2231.6	232.0	743.9
0.985	0.8307	321.4	2163.1	230.8	721.0
0.990	0.8612	319.8	2086.6	229.7	695.5
0.005	0.9013	318.2	1993.7	228.5	664.6
1.000	1.0000	316.6	1796.9	227.4	599.0

UNDER PEER REVIEW

The P_β, V_β values of **765.0 psia** and **233.2 scf/ton** correlate with the experimental isotherm (see **Figure 9**), and the corresponding P_s, V_{max} values of **2294.9 psia** and **324.7 scf/ton** are considered as the developed isotherm parameters for the experimental adsorption data.

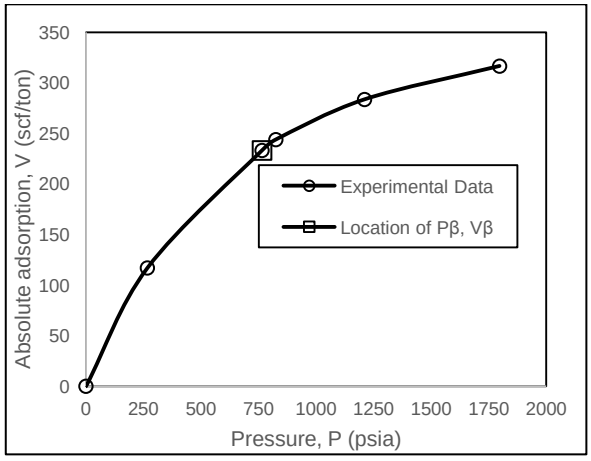

Figure 9: Location of P_β, V_β correlation on the experimental isotherm for pure methane adsorption on dry Tiffany mixed coal sample at 130 ^oF

Hence, pure methane adsorption on dry Tiffany mixed coal sample at 130 ^oF is modelled as:

$$V(scf/ton) = \begin{cases} 324.7\left\{\frac{P}{2294.9} + \left(1 - \frac{P}{2294.9}\right)\left(\frac{P}{2294.9}\right)^{0.50}\right\}, for\ P < 2294.9\ psia \\ 324.7,\ for\ P \geq 2294.9\ psia \end{cases} \quad (48)$$

where maximum adsorbed volume V_{max} = 324.7 scf/ton, adsorption saturation pressure P_s = 2294.9 psia, and n = 0.50 is a parameter that defines dry Tiffany mixed coal sample resistance to pure methane adsorption at 130 ^oF.

Prediction of Methane Adsorption on Dry Tiffany Mixed Coal Sample at 130 ^oF using the Developed Isotherm

Prediction of pure methane adsorption on dry Tiffany mixed coal sample at 130 ^oF using the developed isotherm, and the corresponding deviation (error) analysis parameters are presented in **Table 15** below.

Table 15: Prediction of pure methane adsorption on dry Tiffany mixed coal sample at 130 ^oF using the developed isotherm

Pressure, P (psia)	Absolute adsorption, V (scf/ton)		Deviation (Error) Analysis			
	Experimental	Developed Isotherm	σ_{Exp} (scf/ton)	V_{Cal} - V_{Exp} (scf/ton)	$\frac{V_{Cal} - V_{Exp}}{\sigma_{Exp}}$	$\frac{V_{Cal} - V_{Exp}}{V_{Exp}}$
255.9	117.0	132.5	3.510	15.5	4.416	0.132
824.9	243.9	241.4	7.317	-2.5	-0.342	-0.010
1210.2	283.6	282.7	8.508	-0.9	-0.106	-0.003
1796.9	316.6	316.6	9.498	0	0	0

Here, weighted root mean square, WRMS = 2.2152, weighted average absolute deviation, WAAD = 1.2160, percent average absolute deviation, %AAD = 3.6250, root mean square error, RMSE = 7.8630 scf/ton and R^2 value = 0.9977.

Parameterisation of Pure Methane Adsorption on Dry Tiffany Mixed Coal Sample at 130 ^oF using Langmuir Isotherm

The variation of $^P/_V$ with P for pure methane adsorption on dry Tiffany mixed coal sample at 130 ^oF is shown in **Table 16** and the best fit line of the plot of $^P/_V$ versus P (shown in **Figure 10**) yields the equation: $y = 0.0023x + 1.5619$ with R^2 value of 0.9988, where slope $m = 0.0023 = {}^1/_{V_L}$ and Y-axis intercept $C = 1.5619 = \left(\frac{1}{V_L}\right) P_L$.

Table 16: Parameters for plotting Langmuir isotherm for pure methane adsorption on dry Tiffany mixed coal sample at 130 ^oF

Experimental		$\frac{Pressure}{Volume}$, $^P/_V$
Pressure, P (psiaa)	Absolute adsorption, V (scf/ton)	(psia/scf/ton)
255.9	117.0	2.1872
824.9	243.9	3.3821
1210.2	283.6	4.2673
1796.9	316.6	5.6756

UNDER PEER REVIEW

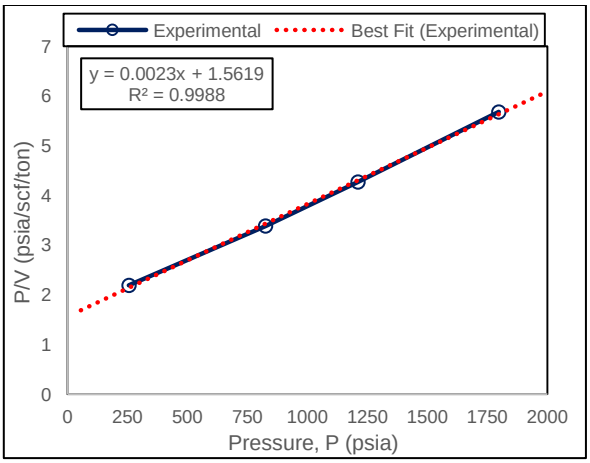

Figure 10: Plot of P/V versus P for pure methane adsorption on dry Tiffany mixed coal sample at 130 ^{o}F

Here, Langmuir volume $\boldsymbol{V_L}$ and Langmuir pressure $\boldsymbol{P_L}$ are respectively obtained as **434.78 scf/ton** and **679.09 psia**. Hence, pure methane adsorption on dry Tiffany mixed coal sample at 130 ^{o}F is modelled as:

$$V(scf/ton) = 434.78\left(\frac{P}{P+679.09}\right) \quad (49)$$

where P is pressure (psia) and Langmuir constant $b = \frac{1}{P_L} = 0.001473$ psia^{-1}.

Prediction of Pure Methane Adsorption on Dry Tiffany Mixed Coal Sample at 130 ^{o}F using Langmuir Isotherm

Prediction of pure methane adsorption on dry Tiffany mixed coal sample at 130 ^{o}F using Langmuir isotherm, and the corresponding deviation (error) analysis parameters are presented in **Table 17** below.

Table 17: Prediction of pure methane adsorption on dry Tiffany mixed coal sample at 130 ^{o}F using Langmuir isotherm

Pressure, P (psia)	Absolute adsorption, V (scf/ton)		Deviation (Error) Analysis			
	Experimental	Langmuir Isotherm	σ_{Exp} (scf/ton)	$V_{Cal} - V_{Exp}$ (scf/ton)	$\frac{V_{Cal} - V_{Exp}}{\sigma_{Exp}}$	$\frac{V_{Cal} - V_{Exp}}{V_{Exp}}$
255.9	117.0	119.0	3.510	2.000	0.570	0.017
824.9	243.9	238.5	7.317	-5.400	-0.738	-0.022
1210.2	283.6	278.5	8.508	-5.100	-0.599	-0.018
1796.9	316.6	315.5	9.498	-1.100	-0.116	-0.003

Here, weighted root mean square, WRMS = 0.5572, weighted average absolute deviation, WAAD = 0.5058, percent average absolute deviation, %AAD = 1.5000, root mean square error, RMSE = 3.8852 scf/ton and R^2 value = 0.9989.

Generalisation of the Developed Isotherm for Pure Methane Adsorption on Dry Tiffany Mixed Coal Sample at 130 ^{o}F

To validate and generalise the developed isotherm, predictions of pure methane adsorption on dry Tiffany mixed coal sample at 130 ^{o}F by Langmuir and the developed isotherms are correlated with the experimental data as shown in **Table 18** and **Figure 11** below.

Table 18: Generalisation of the developed isotherm for pure methane adsorption on dry Tiffany mixed coal sample at 130 ^{o}F

Pressure, P (psia)	Absolute adsorption, V (scf/ton)		
	Experimental	Developed Isotherm	Langmuir Isotherm
255.9	117.0	132.5	119.0
824.9	243.9	241.4	238.5
1210.2	283.6	282.7	278.5
1796.9	316.6	316.6	315.5

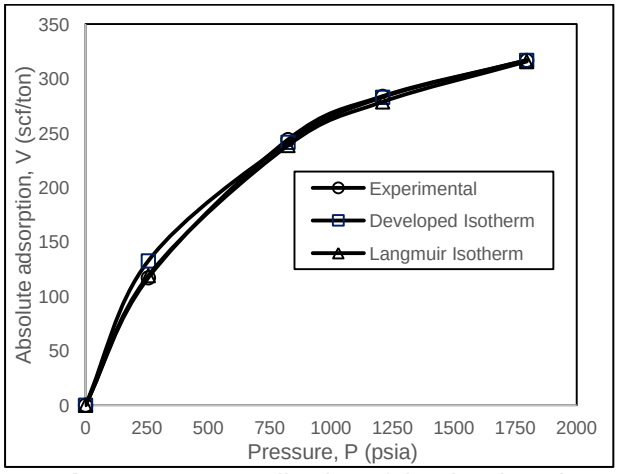

Figure 11: Generalisation of the developed isotherm for pure methane adsorption on dry Tiffany mixed coal sample at 130 ^{o}F

Comparison of High-Pressure Adsorption Prediction for Pure Methane Adsorption on Dry Tiffany Mixed Coal Sample at 130 ^{o}F

Langmuir and the developed isotherms predictions of pure methane adsorption on dry Tiffany mixed coal at 130 ^{o}F for high-pressure range are compared in **Table 19** and **Figure 12** below.

UNDER PEER REVIEW

:

Table 19: Langmuir and the developed isotherms predictions of pure methane adsorption on dry Tiffany mixed coal sample at 130 °F for high-pressure range

Pressure, P (psia)	Absolute adsorption, V (scf/ton)	
	Developed Isotherm	Langmuir Isotherm
255.9	132.5	119.0
824.9	241.4	238.5
1210.2	282.7	278.5
1796.9	316.6	315.5
2294.9	324.7	335.5
2750	324.7	348.7
3250	324.7	359.6
3750	324.7	368.1

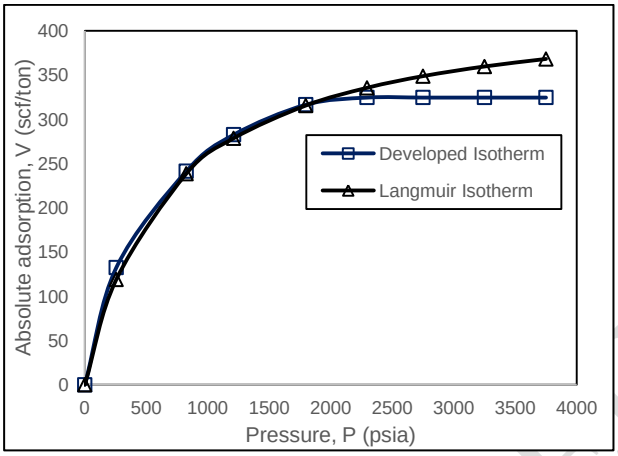

Figure 12: Langmuir and the developed isotherms predictions of pure methane adsorption on dry Tiffany mixed coal sample at 130 °F for large pressure range

The developed isotherm predicts a maximum adsorbed volume of **324.7 scf/ton** at an adsorption saturation pressure of **2294.9 psia**. However, by Langmuir isotherm prediction, a maximum adsorbed volume of **434.78 scf/ton** is attained at an infinite adsorption saturation pressure. **Figure 12** shows that adsorption prediction by Langmuir isotherm is not reliable at higher pressures because of its inefficiency in defining the onset of adsorption saturation pressure; this contributes to an overestimation of maximum adsorbed volume.

COMPETITIVE (GAS MIXTURE) ADSORPTIONS

Methane and Nitrogen (Binary) Adsorptions on Tiffany Mixed Coal Sample at 130 °F

Following the steps of experimental adsorption data parameterisation using the developed isotherm (highlighted above), pure nitrogen adsorption on dry Tiffany mixed coal at 130 °F (see **Table 7**) is modelled as:

$$V\ (scf/ton) = \left\{ 158.3\left\{\frac{P}{2455.7} + \left(1-\frac{P}{2455.7}\right)\left(\frac{P}{2455.7}\right)^{1.00}\right\}, P < 2455.7\ psia \right\} \\ \left\{ 158.3, P \geq 2455.7\ psia \right\} \quad (50)$$

where maximum adsorbed volume $V_{max} = 158.3\ scf/ton$, adsorption saturation pressure $P_s = 2455.7\ psia$, and $n = 1.00$ is a parameter that defines the dry Tiffany mixed coal resistance to pure nitrogen adsorption at 130 °F.

And Langmuir isotherm modelling of the same pure nitrogen adsorption is expressed as:

$$V = 277.78 * \frac{P}{P+1689.92} \quad scf/ton \quad (51)$$

where Langmuir constant $b = \frac{1}{P_L} = 0.0005917\ psia^{-1}$

However, adsorbed gas is often multi-component in nature and each gas competes for the same sorption sites. For methane and nitrogen competitive adsorptions on Tiffany mixed coal sample at 130 °F, the mixing rule for the developed adsorption isotherm (see Equation 40) is correlated with extended Langmuir isotherm (see Equation 41) and validated by the laboratory measurement for the purpose of generalising it.

Adsorption of 50% CH_4 - 50% N_2 on Tiffany Mixed Coal Sample at 130 °F

The laboratory measurement of the competitive adsorption of 50% methane and 50% nitrogen on Tiffany mixed coal sample at 130 °F (Gasem *et al.*, 2002) are shown in **Table 20** and **Figure 13**.

Table 20: Laboratory measurement of the competitive adsorption of 50% methane and 50% nitrogen on Tiffany mixed coal sample at 130 °F

Pressure, P (psia)	$V^{Absolute\ Measured}$ 50% CH_4 (scf/ton)	$V^{Absolute\ Measured}$ 50% N_2 (scf/ton)	$V^{Absolute\ Measured}$ Total (scf/ton)
118.5	37.1	9.3	46.4
220.1	64.5	16.3	80.8
400.0	100.6	24.1	124.7
611.6	130.9	34.1	165.1
813.9	159.1	36.6	195.7
1005.9	177.1	43.3	220.4
1208.5	196.2	44.5	240.7
1409.7	209.5	49.3	258.7
1609.6	223.8	52.8	276.6
1812.8	231.9	60.6	292.5
2010.8	244.9	66.7	311.6

(Source: Gasem *et al.*, 2002)

UNDER PEER REVIEW

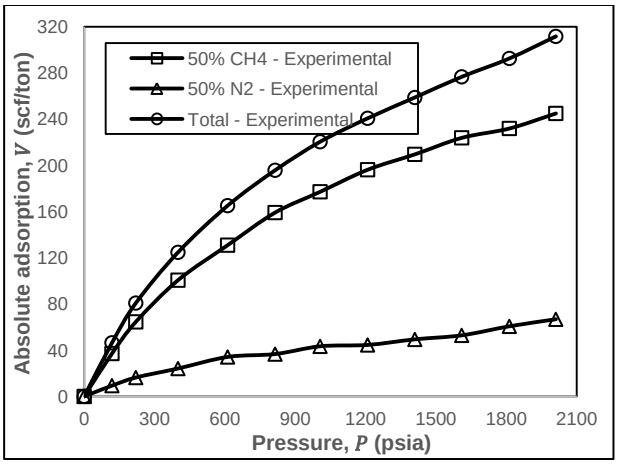

Figure 13: Plot of laboratory adsorption measurement versus pressure for methane and nitrogen competitive adsorption on Tiffany mixed coal sample at 130 ^{o}F

The single-component adsorptions of methane and nitrogen and the corresponding competitive adsorptions on Tiffany mixed coal sample at 130 ^{o}F as predicted by the developed isotherm are shown in **Table 21**. However, **Figure 14** shows the competitive adsorptions as predicted by the developed isotherm.

Table 21: Single-component and competitive adsorption of 50% methane and 50% nitrogen on Tiffany mixed coal sample at 130 ^{o}F as predicted by the developed isotherm

Pressure, P (psia)	**Developed Isotherm**				
	Single Component Adsorption		**Competitive Adsorption**		
	$V^{Absolute}_{Developed\ Isotherm}$ **100% CH_4 (scf/ton)**	$V^{Absolute}_{Developed\ Isotherm}$ **100% N_2 (scf/ton)**	$V^{Absolute}_{Developed\ Isotherm}$ **50% CH_4 (scf/ton)**	$V^{Absolute}_{Developed\ Isotherm}$ **50% N_2 (scf/ton)**	$V^{Absolute}_{Developed\ Isotherm}$ **Total (scf/ton)**
118.5	86.73	14.9	58.3	4.9	63.2
220.1	122.0	27.1	82.0	8.9	90.9
400.0	168.5	47.4	113.3	15.5	128.8
611.6	209.5	69.0	140.4	22.6	163.0
813.9	239.9	87.5	161.7	28.7	190.4
1005.9	263.1	103.1	176.9	33.8	210.7
1208.5	282.5	117.5	189.9	38.5	228.4
1409.7	297.6	129.6	200.1	42.5	242.6
1609.6	308.9	139.5	207.7	45.7	253.4
1812.8	317.1	147.4	213.2	48.3	261.5
2010.8	322.1	153.1	216.5	50.2	266.7

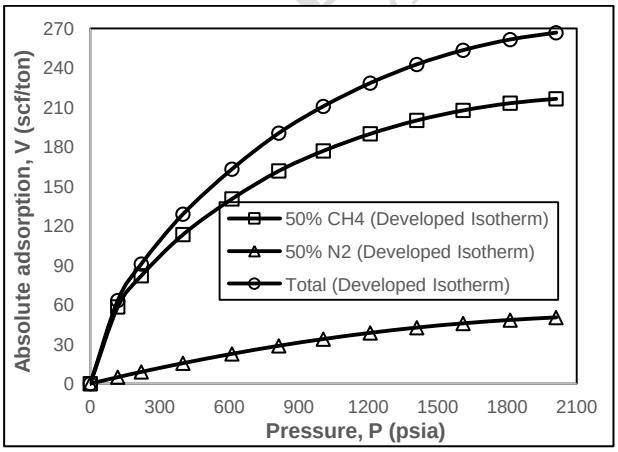

Figure 14: Plot of adsorption versus pressure for methane and nitrogen competitive adsorption on Tiffany mixed coal sample at 130 ^{o}F as predicted by the developed isotherm

Also, the competitive adsorptions of methane and nitrogen on Tiffany mixed coal sample at 130 ^{o}F as predicted by Langmuir isotherm are shown in **Table 22** while the graphical representation is shown in **Figure 15**.

Table 22: Adsorption of 50% methane and 50% nitrogen on Tiffany mixed coal sample at 130 ^{o}F as predicted by Langmuir isotherm

Pressure, P (psia)	$V^{Absolute}_{Langmuir\ Isotherm}$ **50% CH_4 (scf/ton)**	$V^{Absolute}_{Langmuir\ Isotherm}$ **50% N_2 (scf/ton)**	$V^{Absolute}_{Langmuir\ Isotherm}$ **Total (scf/ton)**
118.5	33.8	8.7	42.5
220.1	57.4	14.7	72.1
400.0	90.6	23.3	113.9
611.6	120.0	30.8	150.8
813.9	141.6	36.3	177.9
1005.9	158.0	40.6	198.6
1208.5	172.2	44.2	216.4
1409.7	183.8	47.2	231.0

ER PEER REVIEW

1609.6	193.6	49.7	243.3
1812.8	202.1	51.9	254.0
2010.8	209.3	53.7	263.0

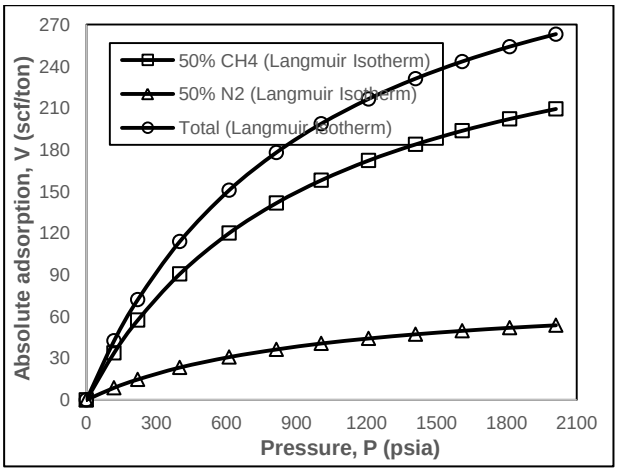

Figure 15: Plot of adsorption versus pressure for methane and nitrogen competitive adsorption on Tiffany mixed coal sample at 130 ^{o}F as predicted by Langmuir isotherm

The correlation of the competitive adsorption prediction of 50% methane and 50% nitrogen on Tiffany mixed coal sample at 130 ^{o}F by the developed isotherm and Langmuir isotherm, and validation by laboratory measurement are graphically shown in **Figure 16**.

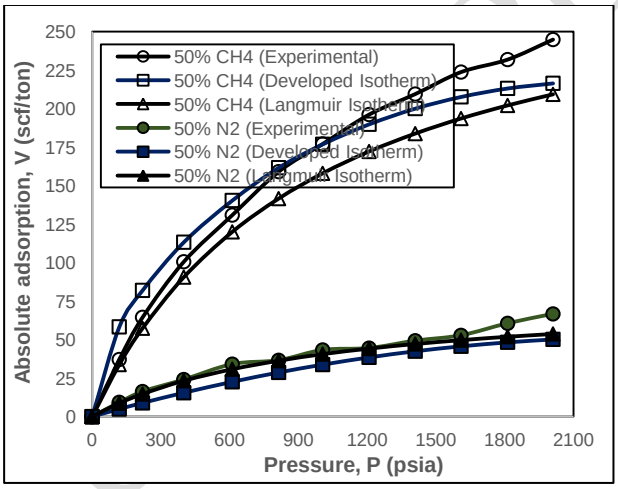

Figure 16: Correlation and validation of the competitive adsorption of 50% methane and 50% nitrogen on Tiffany mixed coal sample at 130 ^{o}F

The plot (**Figure 16**) shows that the developed isotherm prediction of competitive adsorption is better for cases where the adsorbent affinity for the adsorbate is high as displayed in the 50% methane adsorption. However, Langmuir isotherm prediction of competitive adsorption is better for cases where the adsorbent affinity for the adsorbate is low as displayed in the 50% nitrogen adsorption.

CONCLUSION

In this work, a Type-I adsorption isotherm (which assumes a monolayer adsorption like Langmuir isotherm) is developed. The developed isotherm can be used to model all cases of monolayer adsorptions of gases (or fluids) on adsorbents. The developed isotherm discloses and amends the ambiguity surrounding the onset of adsorption saturation pressure in Langmuir isotherm.

The major contributions of the developed isotherm are: (i) offering an effective prediction of low-pressure gas adsorption before the onset of adsorption saturation pressure (P_s), and showing that maximum adsorbed volume (V_{max}) is maintained constant during pressure increase above the adsorption saturation pressure (P_s), (ii) thus revealing and correcting Langmuir isotherm's over-estimation of adsorbed volume at higher pressures, and (iii) showing that Langmuir isotherm could not actually be referred to as a Type I isotherm but a "*pseudo-Type I*" isotherm.

For gas mixture, Langmuir isotherm prediction of competitive adsorption is found to be better for cases where the adsorbent affinity for the adsorbate is low. However, the developed isotherm prediction of competitive adsorption is observed to be better for cases where the adsorbent affinity for the adsorbate is high.

REFERENCES

Adekola F.A., Adegoke H.I. and Ajikanle R.A. (2016), "Kinetic and Equilibrium Studies of Pb(Ii) And Cd(Ii) Adsorption on African Wild Mango (Irvingia Gabonensis) Shell", Bulletin of the Chemical Society of Ethiopia, Vol. 30, No. 2.

Brunauer S., Emmett P.H. and Teller E., (1938), Journal of American Chemical Society, Vol. 6, pp. 309.

Chen L. Jiang Z., Liu K., Ji W., Wang P., Gao F. and Hu T., (2017), "Application of Langmuir and Dubinin–Radushkevich Models to Estimate Methane Sorption Capacity on Two Shale Samples from the Upper Triassic Chang 7 Member in the southeastern Ordos Basin, China", Energy Exploration and Exploitation, Vol. 35, No. 1, pp. 122–144.

Choy K.K., Porter J.F. and McKay G., (2018), "Langmuir Isotherm Models Applied to the Multicomponent Sorption of Acid Dyes from

UNDER PEER REVIEW

Effluent onto Activated Carbon", Journal of Chemical Engineering Data, Vol. 45, No. 4, pp. 575-584.

Dubinin M.M., (1960), "The Potential Theory of Adsorption of Gases and Vapors for Adsorbents with Energetically Non-Uniform Surface", Chem. Rev. 60 (1960) 235–266.

Dubinin M.M., (1966), "Chemistry and Physics of Carbon", in Walker P.L., Ed. Marcel Dekker: New York, Vol. 2, pp. 51-120.

Dubinin M.M. and Astakhov V. A., (1971), "Description of Adsorption Equilibria of Vapors on Zeolites over Wide Ranges of Temperature and Pressure", Advances in Chemistry Series, Vol. 102, pp. 69-85.

Dubinin M.M. and Radushkevich L.V., (1997), "The Equation of the Characteristic Curve of the Activated Charcoal", Proc. Acad. Sci. USSR Phys. Chem. Sect., Vol. 55, pp. 331–337.

Elovich S.Y. and Larinov O.G., (1962), "Theory of Adsorption from Solutions of Non-Electrolytes on Solid (I) Equation Adsorption from Solutions and the Analysis of Its Simplest Form, (II) Verification of the Equation of Adsorption Isotherm from Solutions", Izv. Akad. Nauk. SSSR, Otd. Khim. Nauk, 2, pp. 209–216.

Fowler R.H. and Guggenheim E.A., (1939), "Statistical Thermodynamics", Cambridge University Press, London, pp. 431–450.

Freundlich H.M.F., (1906), "Over the "Adsorption in Solution", J. Phys. Chem. Vol. 57, pp. 385-471.

Gasem K.A.M., Robinson R.L. Jr., and Reeves S.R., (2002), "Adsorption of Pure Methane, Nitrogen, and Carbon Dioxide and their Mixtures on San Juan Basin Coal", DE-FC26-00NT40924 Paper prepared for the U.S. Department of Energy.

Ghiaci M., Abbaspur A., Kia R. and Seyedeyn-Azad F., (2004), "Equilibrium Isotherm Studies for the Sorption of Benzene, Toluene and Phenol onto Organo-zeolites and As-synthesized MCM-41", Sep. Purif. Technol, Vol. 40, pp. 217–229.

Hamzaoui M., Bestani B. and Benderdouche N., (2018), "The Use of Linear and Nonlinear Methods for Adsorption Isotherm Optimization of Basic Green 4-Dye onto Sawdust-Based Activated Carbon", Journal of Materials and Environmental Science, Vol. 9, Issue 4, pp. 1110-1118.

Harkins W.D. and Jura G. J., (1943), Chem. Phys., Vol. 11, pp. 430

IUPAC, 1985.

Jagiello J., Bandosz T.J., Putyera K. and Schwarz J.A., (1995), "Micropore Structure of Template-Derived Carbons Studied using Adsorption of Gases with Different Molecular Diameters", Journal of the Chemical Society, Faraday Transactions, Vol. 91, pp. 2929–2933.

Jin Q., Huang L., Li A. and Shan A., (2017), "Quantification of the Limitation Of Langmuir Model Used In Adsorption Research On Sediments Via Site Energy Heterogeneity", Chemosphere, Vol. 185, pp. 518-528.

Keller J. and Staudt R., (2005). "Gas Adsorption Equilibria: Experimental Methods and Adsorption Isotherms", Springer Science + Business Media, Inc., Boston.

Kiselev A.V., (1958), "Vapor Adsorption in the Formation of Adsorbate Molecule Complexes on the Surface", Kolloid Zhur, Vol. 20, pp. 338–348.

Koble R.A. and Corrigan T.E, (1952), "Adsorption Isotherms for Pure Hydrocarbons", Ind. Eng. Chem., Vol. 44, pp. 383–387.

Kumar K.V. and Sivanesan S., (2007), "Sorption Isotherm for Safranin onto Rice Husk: Comparison of Linear and Non-Linear Methods, Dyes Pigments", Vol. 72, pp. 130–133.

Langmuir I., (1916), "The Constitution and Fundamental Properties of Solids and Liquids", Journal of American Chemical Society, Vol. 38, No 11, pp. 2221-2295.

Mahatmanti F.W., Rengga W.D.P., Kusumastuti E. and Nuryono, (2017), "Adsorption of Pb(II) Ion from Aqueous Solution onto Chitosan/Silica/Polyethylene Glycol (Ch/Si/P) Composites Membrane", IOP Conference Series: Materials Science and Engineering, United Kingdom.

Malek A. and Farooq S., (1996),"Comparison of Isotherm Models for Hydrocarbon Adsorption on Activated Carbon", American Institute of Chemical Engineers Journal. Vol. 42, No. 11, pp. 3191–3201.

UNDER PEER REVIEW

Markham E.D. and Benton A.F., (1931), "The Adsorption of Gas Mixtures by Silica", J. Am. Chem. Soc., Vol. 53, pp. 497.

Merey S., (2013), "Experimental Analysis of Adsorption Capacities and Behaviors of Shale Samples', M.Sc Thesis, Middle East Technical University, Turkey.

Myers A.L. and Prausnitz J.M., (1965), "Thermodynamics of Mixed-Gas Adsorption", AIChE Journal, Vol. 11, No. 1, pp. 121-127.

Moore W.J., (1972), Physical Chemistry, Prentice-Hall, Inc

Nitta T., Shigetomi T., Kuro-Oka M. and Katayama T., (1984), "An Adsorption Isotherm of Multi-Site Occupancy Model for Homogeneous Surface", Journal of Chemical Engineering of Japan, Vol. 17, No. 1, pp. 39-45

Redlich O. and Peterson D.L., (1959), "A Useful Adsorption Isotherm", J. Phys. Chem., Vol. 63, pp. 1024–1026

Sips R., (1948), "Combined Form of Langmuir and Freundlich Equations", J. Chem. Phys., Vol. 16, pp. 490–495.

Temkin M.I. and Pyzhev V., (1940), "Kinetics of Ammonia Synthesis on Promoted Iron Catalyst", Acta Phys. Chim. USSR, Vol. 12, pp. 327–356.

Toth J., (1971), "State Equations of the Solid Gas Interface Layer, Acta Chem. Acad. Hung., Vol. 69, pp. 311–317.

3-Legs Resources, 2011

APPENDICES

Appendix A

Derivation of Langmuir Isotherm: Kinetic Approach

Langmuir isotherm describes a progressively increasing surface adsorption as a function of pressure up until the entire surface area is covered with a single layer of molecules and no further adsorption can occur (see **Figure 1**).

Considering fluid phase F, vacant surface sites $[S]$, and occupied surface sites $[F_{ads}]$ (number/area); the rates of adsorption and desorption of fluid molecules are R_{ads} and R_{des} respectively.

Rate of adsorption is proportional to the partial pressure P_f of the fluid over the surface and the concentration of vacant sites $[S]$ (number/area):

$$R_{ads} = K_{ads} \cdot P_f \cdot [S] \quad \text{(A.1)}$$

where K_{ads} is adsorption rate coefficient.

Rate of desorption is proportional to the concentration of sites filled with fluid molecules $[F_{ads}]$ (number/area):

$$R_{des} = K_{des} \cdot [F_{ads}] \quad \text{(A.2)}$$

where K_{des} is desorption rate coefficient.

If adsorption coverage is assumed to be independent of the enthalpy of adsorption, then the dynamic equilibrium parameter K_{eq}^{f} has a constant value and it is referred to as Langmuir dynamic equilibrium constant.

At dynamic equilibrium, rate of adsorption equals rate of desorption. Hence,

$$K_{eq}^{f} = \frac{K_{ads}}{K_{des}} = \frac{[F_{ads}]}{P_f \cdot [S]} \quad \text{(A.3)}$$

Concentration of all sites $[S_T]$ is the sum of the concentrations of vacant and occupied sites (number/area):

$$[S_T] = [S] + [F_{ads}] \quad \text{(A.4)}$$

With reference to (A.3),

$$[S_T] = \frac{[F_{ads}]}{K_{eq}^{f} \cdot P_f} + [F_{ads}] \quad \text{(A.5)}$$

$$[S_T] = [F_{ads}] \left\{ \frac{1 + K_{eq}^{f} \cdot P_f}{K_{eq}^{f} \cdot P_f} \right\} \quad \text{(A.6)}$$

The fraction of the surface sites occupied by fluid $[F]$ is defined as:

$$\theta = \frac{[F_{ads}]}{[S_T]} \quad \text{(A.7)}$$

Hence,

$$\theta = \frac{[F_{ads}]}{[S_T]} = \frac{K_{eq}^{f} \cdot P_f}{1 + K_{eq}^{f} \cdot P_f} \quad \text{(A.8)}$$

Expressing the partial pressure P_f as P, the occupied surface site $[F_{ads}]$ as the volume of fluid adsorbed V_{ads}, the concentration of all sites $[S_T]$ as the Langmuir volume V_L, (the maximum fluid adsorbable), and the Langmuir dynamic equilibrium constant K_{eq}^{f} as b; the fractional loading of the surface sites is then expressed as:

$$\theta = \frac{V_{ads}}{V_L} = \frac{bP}{1 + bP} \quad \text{(A.9)}$$

$$V_{ads} = V_L \cdot \frac{bP}{1 + bP} \quad \text{(A.10)}$$

Equation (A.10) is the Langmuir adsorption isotherm where b is the Langmuir dynamic equilibrium constant determined as $\frac{1}{P_L}$ and P_L is the Langmuir pressure (the pressure at a volume $\frac{V_L}{2}$).

UNDER PEER REVIEW

Therefore, Langmuir isotherm could be expressed as:

$$V_{ads} = V_L \cdot \frac{P}{P+P_L} \quad \text{(A.11)}$$

Appendix B

Derivation of Pressure P_β and Adsorbed Volume V_β at Inflexion Point β where $\Delta\left(\frac{V}{V_{max}}\right) = \Delta\left(\frac{P}{P_s}\right)$ on the Developed Isotherm

With reference to **Equation 14**,

$$\frac{dP_a}{dP} = \frac{d}{dP}\left\{(P_s - P)\left(\frac{P}{P_s}\right)^n\right\} \quad \text{(B.1)}$$

$$\frac{dP_a}{dP} = \frac{d}{dP}\left\{\left(\frac{P_s}{{P_s}^n}\right)P^n - \left(\frac{1}{{P_s}^n}\right)P^{n+1}\right\} \quad \text{(B.2)}$$

$$\frac{dP_a}{dP} = n\left(\frac{P_s}{{P_s}^n}\right)P^{n-1} - (n+1)\left(\frac{1}{{P_s}^n}\right)P^n \quad \text{(B.3)}$$

However, $\frac{dP_a}{dP} = 0$ at inflexion point β where $\Delta\left(\frac{V}{V_{max}}\right) = \Delta\left(\frac{P}{P_s}\right)$ on the developed isotherm. Hence, at pressure P_β,

$$n\left(\frac{{P_\beta}^n}{{P_s}^n}\right)\left(\frac{P_s}{P_\beta}\right) = (n+1)\left(\frac{{P_\beta}^n}{{P_s}^n}\right) \quad \text{(B.4)}$$

$$n\left(\frac{P_s}{P_\beta}\right) = (n+1) \quad \text{(B.5)}$$

$$P_\beta = \left(\frac{n}{n+1}\right)P_s \quad \text{(B.6)}$$

and

$$V_\beta = V_{max}\left\{\frac{P_\beta}{P_s} + \left(1 - \frac{P_\beta}{P_s}\right)\left(\frac{P_\beta}{P_s}\right)^n\right\} \quad \text{(B.7)}$$

UNDER PEER REVIEW